Molecular Imaging and Biology
https://doi.org/10.1007/s11307-025-02073-6

RESEARCH ARTICLE

Ethyl Pyruvate Promotes Wound Healing in Elastase-Induced Lung Injury in Mice as Assessed by Hyperpolarized ^{129}Xe Magnetic Resonance Imaging

Atsuomi Kimura[1] · Akihiro Shimokawa[1] · Neil J. Stewart[2] · Rie Hosoi[1] · Hirohiko Imai[3] · Hideaki Fujiwara[1]

Received: 29 May 2025 / Revised: 16 October 2025 / Accepted: 1 December 2025

Abstract

Purpose Wound healing process in lung injury involves the activation of the mitogen-activated protein kinase (MAPK) pathway. In this study, we investigated the role of the MAPK pathway in wound healing in a murine model of emphysema using hyperpolarized ^{129}Xe (HP ^{129}Xe) magnetic resonance imaging (MRI).

Procedures Porcine pancreatic elastase was administered intratracheally to 25 mice to induce lung injury. Temporal changes in pulmonary gas exchange function were monitored using HP ^{129}Xe MRI, revealing a significant decline in function one day after elastase administration. Treatments with ethyl pyruvate (EP) and nicorandil (Nic), which upregulate and downregulate the MAPK pathway, respectively, were initiated in 12 and 7 of the 25 mice, respectively, and continued for 20 days. Over the 21-day period, HP ^{129}Xe MRI was performed to monitor the disease progression and treatment efficacy through changes in the metrics of gas exchange and fractional ventilation.

Results HP ^{129}Xe MRI showed that EP significantly improved gas exchange function 14 days after elastase administration, whereas Nic did not show any improvement. Ventilatory function also improved in the EP group, but not in the Nic group, 14 days after elastase administration. Histological analysis showed that EP repaired tissue damage to a level similar to that observed in healthy mice, whereas Nic did not.

Conclusions In the present study, we provide some insight into the role of the MAPK pathway in wound healing in elastase-induced lung injury, as assessed using the HP ^{129}Xe MRI protocol.

Key words Hyperpolarized ^{129}Xe magnetic resonance imaging · Elastase-induced lung injury · Mitogen-activated protein kinase · Ethyl pyruvate · Nicorandil

Introduction

Hyperpolarized ^{129}Xe (HP ^{129}Xe) magnetic resonance imaging (MRI) is an established tool for clinically imaging pulmonary function [1–3]. This method has been applied for the functional assessment of various lung diseases in humans [4]. In a previous study, we developed a unique continuous-flow type HP ^{129}Xe polarizer and applied it to murine pulmonary functional imaging under spontaneous breathing, which allowed us to evaluate pulmonary function under natural conditions [5, 6]. Recently, we have utilized our HP ^{129}Xe MRI preclinical evaluation system to identify therapeutic drugs for several lung diseases [7–10]. Ethyl pyruvate (EP) was shown to be effective in repairing lung tissue and improving pulmonary function damaged by diseases such as chronic obstructive pulmonary disease (COPD), pulmonary fibrosis, and lung cancer [8–10].

A hallmark of lung diseases is the involvement of high mobility group box 1 (HMGB1), a damage-associated molecular pattern molecule, in disease progression [11–14]. Upon lung injury, HMGB1 is released from macrophages and cells undergoing apoptosis or necrosis, which binds to

✉ Atsuomi Kimura
kimura@sahs.med.osaka-u.ac.jp

1 Division of Health Sciences, Graduate School of Medicine, The University of Osaka, 1-7 Yamadaoka, Suita, Osaka 565-0871, Japan

2 Division of Clinical Medicine, School of Medicine & Population Health, Faculty of Health, POLARIS, University of Sheffield, Sheffield, UK

3 Innovation Research Center for Quantum Medicine, Gifu University School of Medicine, 1-1 Yanagido, Gifu 501-1194, Japan

Published online: 10 December 2025

Toll-like receptor 4 (TLR4) and the receptor for advanced glycation end products (RAGE), which are highly expressed in alveolar epithelial cells [14, 15]. After binding to TLR4, HMGB1 activates the transcription factor nuclear factor kappa B (NF-κB) and induces inflammatory responses [16]. Furthermore, after binding to RAGE, HMGB1 generates reactive oxygen species (ROS) in the cytoplasm [17], and these ROS activate the mitogen-activated protein kinase (MAPK) signaling pathway in addition to the NF-κB pathway, exacerbating the pathology [18, 19].

In contrast, moderate activation of extracellular signal-regulated kinases (ERK) (1/2), which are involved in the MAPK pathway, has been reported to be paradoxically involved in wound healing in skin disorders and diabetes-induced tissue damage [20–22]. Overexpression of HMGB1 has been shown to aggravate the pathology of lung diseases [15, 23], whereas EP has been reported to downregulate HMGB1 production, deactivate NF-κB, and upregulate the expression of ERK(1/2) in a dose-dependent manner [24–26]. EP has also been reported to increase intracellular ROS and activate ERK to inhibit melanogenesis in B16F10 melanoma cells for the treatment of hyperpigmentation disorders [27].

Here, we hypothesize that EP modulates the expression levels of HMGB1 and intracellular ROS, deactivate NF-κB, and moderately activates the MAPK/ERK pathway to exert coordinated anti-inflammatory and tissue repair effects and improve pulmonary function. In this study, we attempted to confirm this hypothesis by observing the treatment response to EP in elastase-induced acute lung injury using HP ^{129}Xe MRI. To the best of our knowledge, there have been no reports on the application of EP in the treatment of elastase-induced lung injury. The treatment response of EP was compared with that of nicorandil (Nic), which exhibits its protective effect against lung injury through suppression of ROS production and downregulation of the NF-kB and MAPK pathways [28].

Materials and Methods

Ethics Statement

The animal study protocol was approved by the Institutional Animal Care and Use Committee of Division of Health Sciences, Graduate School of Medicine, The University of Osaka (approval no. 24–03-03).

Animal Preparation

A total of 33 mice, 6-week-old, male ddY mice (Japan SLC Ltd., Hamamatsu, Japan) were divided into four groups: (i) sham-instilled group ($n=8$), (ii) porcine pancreatic elastase (PPE)-treated group ($n=6$), (iii) EP-treated group ($n=12$), and (iv) Nic-treated group ($n=7$). Sham-instilled mice were administered 40 µL of saline intra-tracheally for five consecutive days per week for 21 days. A saline solution of PPE (40 µL, 300 U/kg body weight; FUJIFILM Wako Pure Chemical Corporation, Osaka, Japan) was intra-tracheally administered to each mouse in the PPE-, EP-, and Nic-treated groups to induce lung injury (the day of PPE administration was set as day 0). One day after PPE administration, EP and Nic treatments were initiated in the EP- and Nic-treated groups, respectively, following a similar protocol as previously reported [9]. In brief, a 40 µL saline solution of EP (2.6 mg/kg body weight; Tokyo Chemical Industry Ltd, Tokyo, Japan) or Nic (2.4 mg/kg body weight; BIOMOL International, Pennsylvania, USA) was intra-tracheally administered to each mouse in the EP- or Nic-treated group for five consecutive days per week for a 20-day period. The PPE-treated mice were intra-tracheally administered with 40 µL saline solution for five consecutive days per week for a 20-day period. In all cases, prior to instillation, the mice were anesthetized with 5% isoflurane (ISOFLU®, Dainippon Sumitomo Pharmaceutical Co. Ltd, Osaka, Japan). The survival rate of the 21-day procedure was 100% in all groups.

MRI measurements of sham-instilled mice were conducted on day 0. PPE was administered to each mouse in the EP-, Nic-, and PPE-treated groups on day 0, as described above. One day after PPE administration, MRI measurements were performed for the EP-, Nic-, and PPE-treated groups. During the remaining of the 20-day period, MRI measurements were performed on days 7, 14, and 21 after PPE administration for all groups. A home-built glass mask was attached to the mouth of each mouse to deliver HP ^{129}Xe and oxygen and remove exhaust gases. For respiratory-gated imaging, a pulse transducer (AD Instruments Ltd., Dunedin, New Zealand) was positioned on the abdomen of each mouse to synchronize image acquisition with the respiratory motion of spontaneously breathing mice. During MRI measurements, mice were anesthetized with 2% isoflurane, and their body temperature was maintained using warm water circulating through a rubber tube placed on the abdomen. The animal breathing rate was approximately 150 breaths/min. The MR imaging procedure was performed without tracheal intubation or tracheotomy, and hence it was entirely noninvasive.

MRI Measurements

All MRI measurements were performed using Agilent Unity INOVA 400 WB spectrometer (Agilent Technologies, Inc., Santa Clara, CA, USA) with a 9.4 T vertical magnet (Oxford Instruments Plc., Oxford, UK) and a Highland L-500 Gradient Amp system (Highland Technology, Inc. California, USA). A self-shielded imaging probe with a Litz coil

switchable to ^{129}Xe and ^{1}H frequencies, 32-mm in diameter and 15-mm in length (Clear Bore DSI-1117; Doty Scientific, Inc., Columbia, SC, USA) was used.

High-purity xenon gas (> 99.995%) with ^{129}Xe in its natural abundance, 26.4%, mixed with nitrogen (Japan Air Liquide, Tokyo, Japan) was used to produce HP ^{129}Xe for MRI measurements using a home-built continuous-flow type apparatus [5–10]. A gas mixture containing HP ^{129}Xe and N_2 (70% HP ^{129}Xe and 30% N_2) was continuously supplied to mice placed in NMR probe at a rate of 50 ml/min through a mask attached to their head. In the mask, O_2 (Japan Air Liquide, Tokyo, Japan) was mixed with Xe/N_2 gas mixture at a rate of 12 ml/min immediately prior to inhalation. The mice spontaneously inhaled a 56:24:20 volume mixture of Xe:N_2:O_2 gases.

Assessment of Pulmonary Function

The pulmonary function of gas exchange metric f_D (%), the rate of HP ^{129}Xe magnetization diffusing from the gas phase (alveolar air space) to the dissolved phase (alveolar tissue and blood) within a given exchange time, was assessed from HP ^{129}Xe MR images acquired using a balanced steady-state free precession (bSSFP) sequence, as described previously [7, 9]. A parametric map of f_D for each mouse was obtained via pixel-by-pixel analysis using MATLAB (MathWorks, Inc., Natick, MA, USA). The map was then averaged to obtain the whole lung f_D value. The measurements were repeated three times, and the obtained f_D values were averaged.

Similarly, the fractional ventilation r_a, the alveolar volume fraction of gas turned over in a single breath, was also assessed [7, 9]. A parametric map of r_a and whole lung r_a value were derived using the same process as for f_D, and mean r_a values were compared between the groups.

Acquisition parameters of HP ^{129}Xe images were as follows: 1000-μs Gaussian-shaped radiofrequency (RF) pulse of flip angle θ = 40º; acquisition bandwidth, 88 kHz; TR/TE = 3.6 ms/1.8 ms; echo train length, 8; number of shots, 4; number of averages, 8; coronal slice thickness, 20 mm; number of slices, 1; matrix, 64 × 32 with a field of view of 80 × 25 mm^2. Acquisition was commenced after confirming a steady state signal by monitoring ^{129}Xe MR spectra obtained by the application of an 8º hard RF pulse with an interval of 2 s.

Histology

After completion of MRI experiments, the mice were euthanized with a lethal dose of carbon dioxide gas. Lungs were extracted, fixed in 10% formalin, and processed for histological examination by staining with hematoxylin and eosin (H&E), as previously described [7]. Four coronal slices taken close to the center of the lungs per mouse were captured using a digital microscope (Celestron LCD Microscope PRO < CE44345 >; Celestron, LLC., Torrance, CA, USA). The captured images were used to evaluate the mean linear intercept (MLI) and mean bronchial wall thickness ($h_{bw\_histology}$). The MLI and $h_{bw\_histology}$ values were determined from five regions of the lung (right upper lobe, right middle lobe, right lower lobe, and the upper and lower lobes of the left lung). Each set of five values was averaged over the four slides, and the resulting five averaged regional MLI and $h_{bw\_histology}$ values were averaged to yield a single mean MLI and $h_{bw\_histology}$ value for each mouse of the sham-instilled, PPE- and EP-, and Nic-treated groups.

Statistical Analysis

The f_D, r_a and MLI values were compared among the four mouse groups using the Kruskal–Wallis test. When any significant differences were detected, pairwise comparisons were performed using the Mann–Whitney U test. All of the data are presented as mean ± standard error and/or box-and-whisker plots, and differences in signal intensities were considered significant at $P < 0.05$.

Results

Temporal Changes in Pulmonary Gas Exchange Function

Temporal changes in representative f_D parametric maps and f_D values for the sham-instilled, PPE-, EP-, and Nic-treated groups are illustrated in Fig. 1a and 1b, respectively. Notably, EP and Nic treatments were initiated one day after PPE administration (set as day 0). When compared with the f_D of the sham-instilled group on day 0 ($f_{D\_sham\text{-}instilled} = 6.8 \pm 0.7\%$), significant decrease in the f_D values of the PPE- ($f_{D\_PPE\text{-}treated} = 5.1 \pm 0.4\%$), EP- ($f_{D\_EP\text{-}treated} = 4.4 \pm 1.2\%$), and Nic-treated ($f_{D\_Nic\text{-}treated} = 4.8 \pm 0.8\%$) groups was observed on day 1 after PPE administration ($P < 0.01$). Significant decrease in the f_D value of the PPE-treated group compared with that of the sham-instilled group was consistent for 21 days after PPE administration. Similarly, decrease in the f_D values of both EP- and Nic-treated groups was observed until day 7 after PPE administration. However, the f_D value of the EP-treated group recovered to a similar level as that of the sham-instilled group on day 14 after PPE administration ($f_{D\_sham\text{-}instilled} = 6.9 \pm 0.6\%$ and $f_{D\_EP\text{-}treated} = 6.6 \pm 0.9\%$), but was significantly higher than that of the PPE and Nic groups ($f_{D\_PPE\text{-}treated} = 4.0 \pm 1.2\%$ and $f_{D\_Nic\text{-}treated} = 4.9 \pm 1.0\%$, $P < 0.01$). This recovery continued until day 21. However,

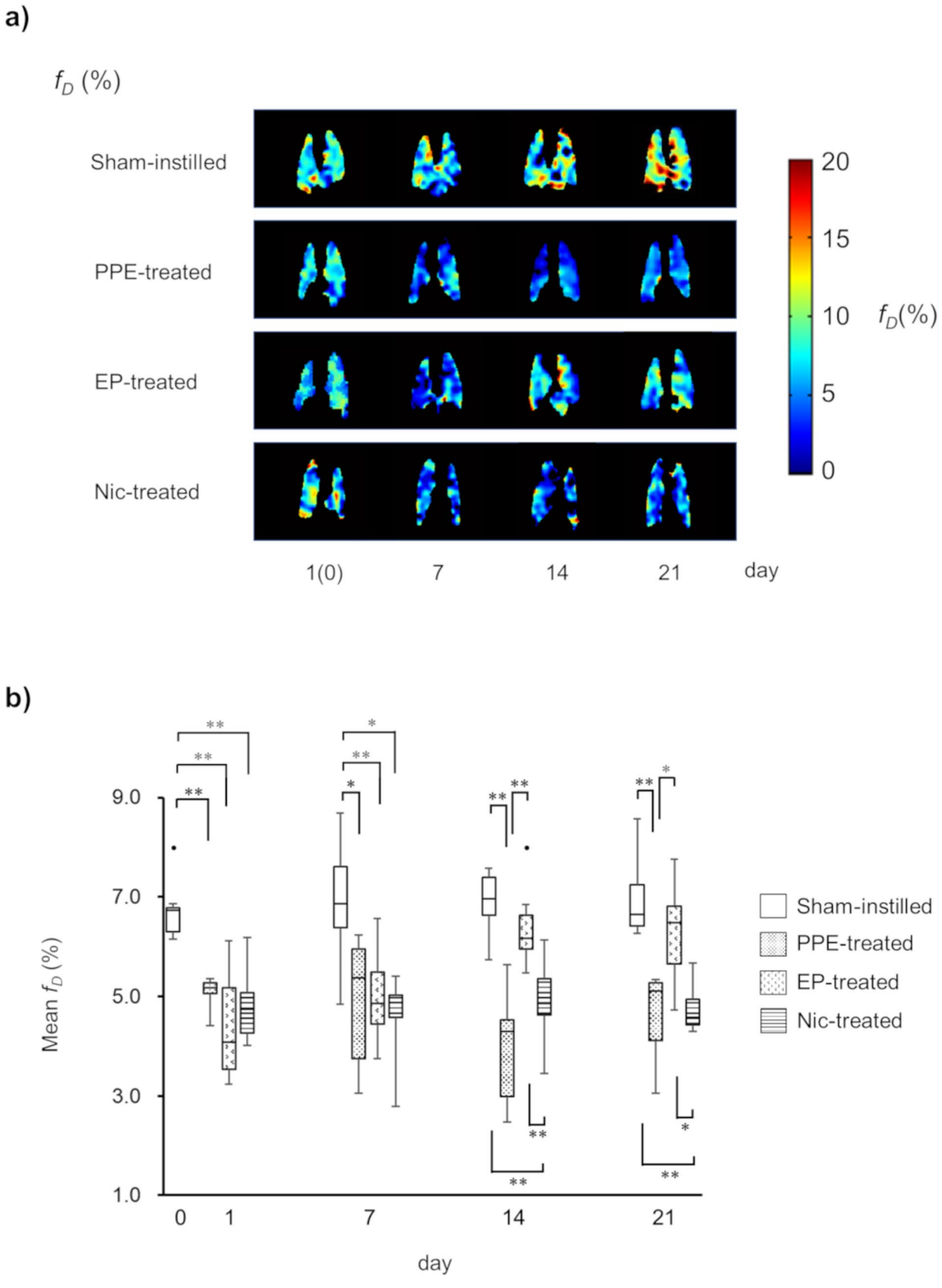
a)
f_D (%)
Sham-instilled
PPE-treated
EP-treated
Nic-treated
20
15
10
5
0
f_D(%)
1(0)
7
14
21
day
b)
Mean f_D (%)
9.0
7.0
5.0
3.0
1.0
0
1
7
14
21
day
Sham-instilled
PPE-treated
EP-treated
Nic-treated

◂**Fig. 1** Temporal changes in representative f_D parametric maps of mice of each of the four groups, from top to bottom: sham-instilled; PPE-treated; EP-treated; Nic-treated (**a**). Box plots of temporal changes in the mean f_D values for all mice, separated by groups (**b**). The time course from the initial intra-tracheal injection of saline or PPE is shown horizontally. Significant differences between groups are indicated by solid lines (*: $P<0.05$, **:$P<0.01$). Of note, EP and Nic treatments were initiated one day after PPE administration on day 0. The first f_D map of sham-instilled mouse was obtained from day 0, whereas the first maps of PPE-, EP-, and Nic-treated mice were obtained from day 1

the f_D value of the Nic group did not recover over the remaining period.

Temporal Changes in Pulmonary Ventilation Function

Temporal changes in the representative r_a parametric maps and r_a values of the sham-instilled, PPE-, EP-, and Nic-treated groups are shown in Fig. 2a and b, respectively. In contrast to the results of f_D measurements, the r_a values of the PPE- ($r_{a\_\text{PPE-treated}}=0.20\pm0.06$), EP- ($r_{a\_\text{EP-treated}}=0.20\pm0.05$), and Nic-treated ($r_{a\_\text{Nic-treated}}=0.19\pm0.07$) groups were not decreased on day 1 after PPE administration compared with the r_a value of the sham-instilled group on day 0 ($r_{a\_\text{sham-instilled}}=0.27\pm0.02$). This tendency persisted until day 7. On day 14, the r_a values of the PPE- ($r_{a\_\text{PPE-treated}}=0.18\pm0.06$) and Nic-treated ($r_{a\_\text{Nic-treated}}=0.17\pm0.03$) groups were significantly decreased compared with that of the sham-instilled group ($r_{a\_\text{sham-instilled}}=0.25\pm0.02$, $P<0.05$). On the other hand, the r_a value of the EP-treated group ($r_{a\_\text{EP-treated}}=0.23\pm0.03$) was found to be significantly higher than that of the Nic-treated group on day 14 ($P<0.05$). On day 21, the r_a value of the EP-treated group ($r_{a\_\text{EP-treated}}=0.23\pm0.02$, $P<0.01$) was significantly increased when compared with that of the sham-instilled group($r_{a\_\text{sham-instilled}}=0.23\pm0.02$, $P<0.01$) and that of the Nic-treated group ($r_{a\_\text{Nic-treated}}=0.19\pm0.03$).

Histograms of Pulmonary Gas Exchange Function

Figure 3 shows the comparative results of representative histograms of f_D values obtained from f_D maps of a sham-instilled mouse on day 0, a PPE-treated mouse on day 1, and a PPE-treated mouse on day 21.

Histology

Representative histological images obtained from mice of the sham-instilled, PPE-, EP-, and Nic-treated groups are shown in Fig. 4a. The whole lung mean MLI values obtained from the sham-instilled, PPE-, EP-, and Nic-treated groups are shown in Fig. 4b. As illustrated in Fig. 4a, alveolar enlargement was observed in the PPE- and Nic-treated groups. The mean MLI of the PPE-treated group ($MLI_{PPE\text{-}treated}=46.3\pm9.4$ μm) was significantly higher than that of the sham-instilled and EP-treated groups ($MLI_{Sham\text{-}instilled}=38.0\pm2.0$ μm and $MLI_{EP\text{-}treated}=37.8\pm5.6$ μm, $P<0.05$). The MLI of the Nic-treated group ($MLI_{Nic\text{-}treated}=42.8\pm2.7$ μm) was not significantly different from that of the sham-instilled, PPE-, and EP-treated groups.

Representative histological images and whole lung mean $h_{bW\_histology}$ values obtained from mice of the sham-instilled, PPE-, EP-, and Nic-treated groups are shown in Fig. 5. There were no significant differences in $h_{bW\_histology}$ values between the groups.

Mechanisms of Therapeutic Effect of EP and Nic

Figure 6 depicts the mechanisms underlying the therapeutic effect of EP (Fig. 6a) and Nic (Fig. 6b) against the elastase-induced lung injury proposed in this study.

Discussion

In the present study, we successfully monitored the temporal changes in pulmonary function, f_D and r_a, induced by PPE administration using HP ^{129}Xe MRI (Figs. 1 and 2). One day after PPE administration, the f_D values of the PPE-, EP-, and Nic-treated groups were significantly lower than that of the sham-instilled group on day 0 (Fig. 1). Emphysema was previously reported to develop seven days after PPE administration [29]. Therefore, our data suggest that the f_D metric can detect changes in pulmonary function due to pathology before emphysema development. This observation is similar to that of our previous study using a mouse model of lung cancer, in which inflammation-induced alveolar septal wall thickening reduced f_D values prior to the onset of lung cancer [10]. On the other hand, one day after PPE administration, no significant changes were observed in the r_a values of the PPE-, EP-, and Nic-treated groups compared with that of the sham-instilled group on day 0 (Fig. 2). In our previous study, we reported that inflammation-induced bronchial wall thickening reduced r_a values [7]. In the present study, bronchial wall thickening was not observed in any histological images of the PPE-, EP-, or Nic-treated groups compared with those of the sham-instilled group (Fig. 5), suggesting no changes in r_a values were observed one 1 day after PPE administration.

Considering the above observations, although no alveolar septal wall thickening was observed histologically 21 days after PPE administration (Fig. 4), we assumed that alveolar septal wall thickening might occur without bronchial wall thickening due to inflammation on day 1 after PPE administration, before the onset of emphysema. Previously, using

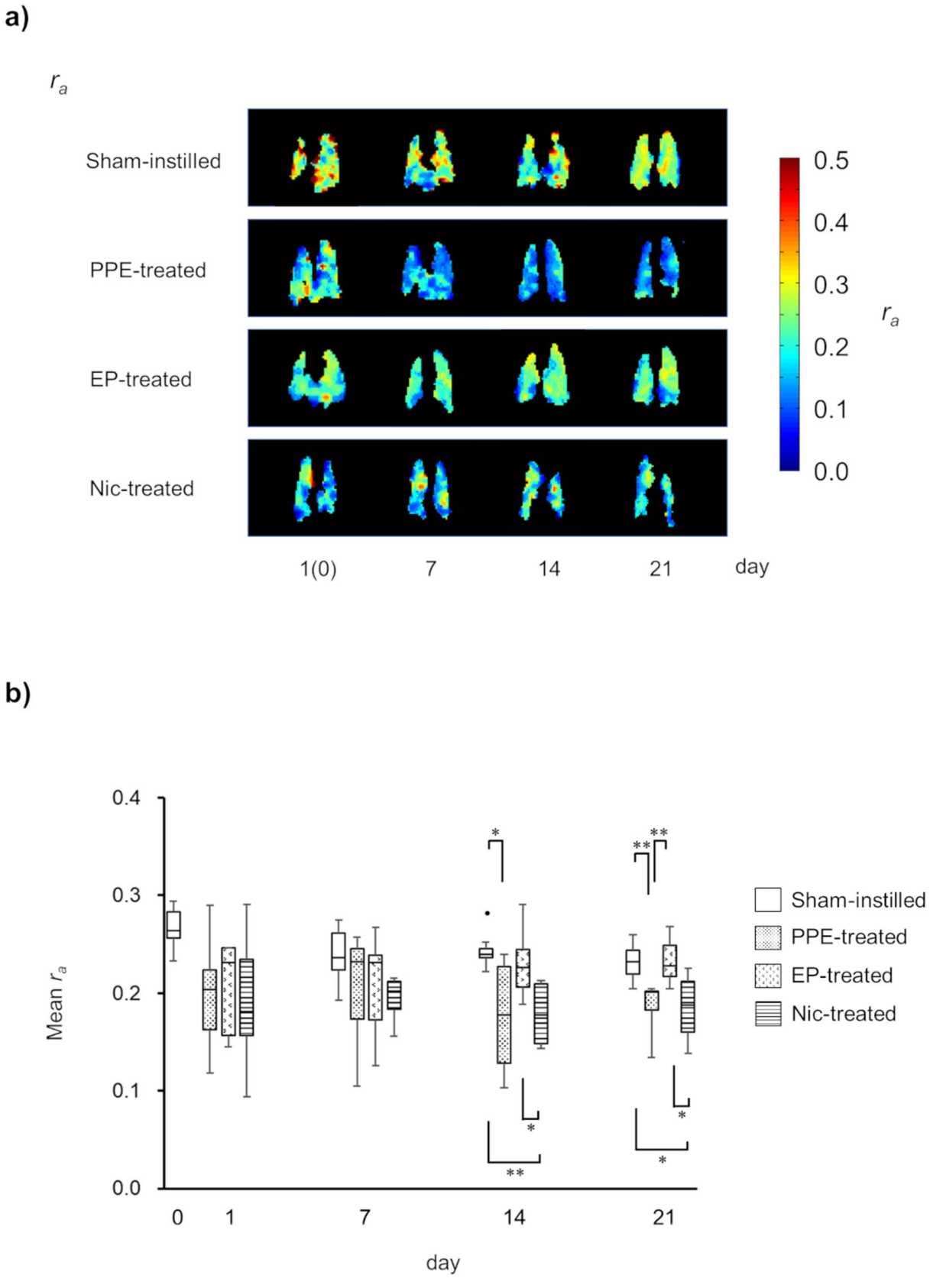

Fig. 2 Temporal changes in representative r_a parametric maps of mice of each of the four groups, from top to bottom: sham-instilled; PPE-treated; EP-treated; Nic-treated (**a**). Box plots of temporal changes in the mean r_a values for all mice, separated by groups (**b**)

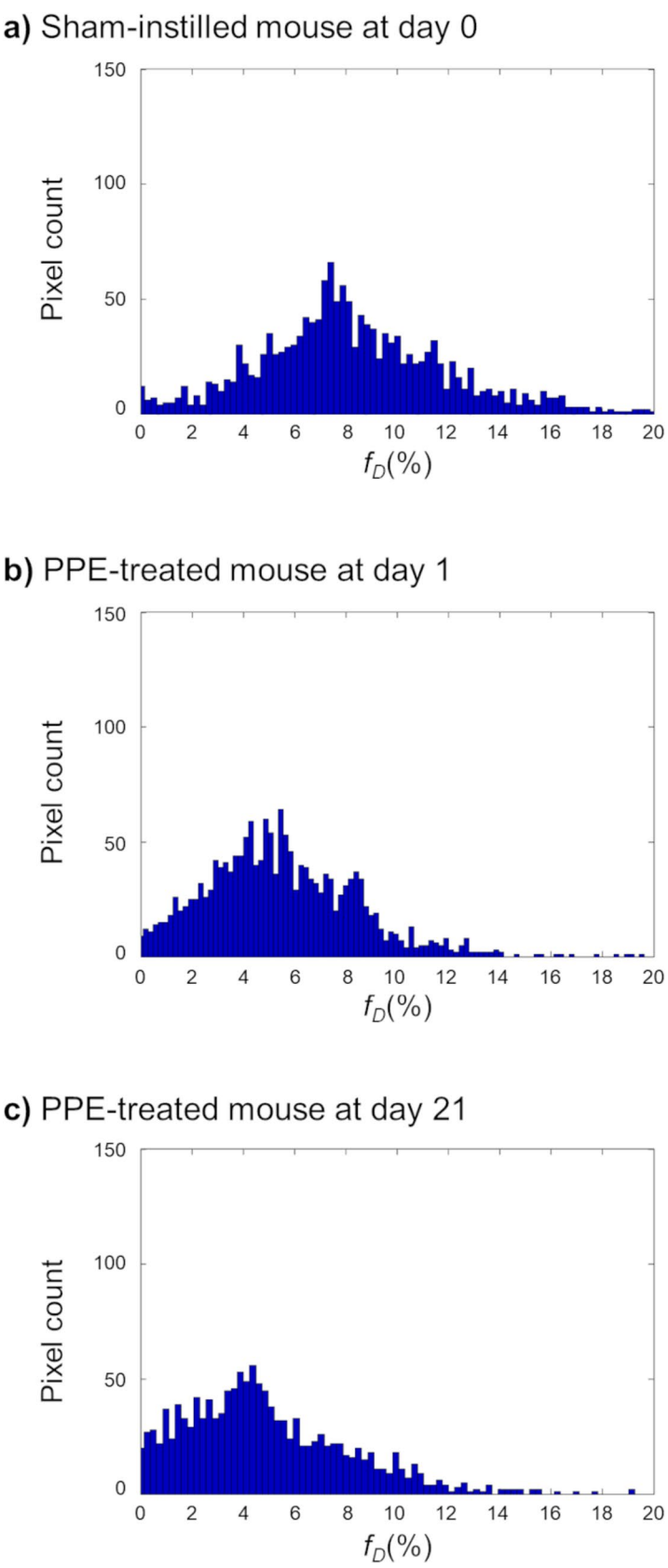

Fig. 3 Representative histograms of f_D values obtained from sham-instilled mice (**a**), PPE-treated mice on day 1 (**b**), and PPE-treated mice on day 21 (**c**). The global mean $f_D = 7.2\%$ (**a**), 5.1% (**b**), and 4.9% (**c**). After PPE injection, f_D values tended to shift to lower values without a decrease in the total area of the histogram, suggesting regional transfer from higher f_D sites to lower f_D sites as a result of the pathological process

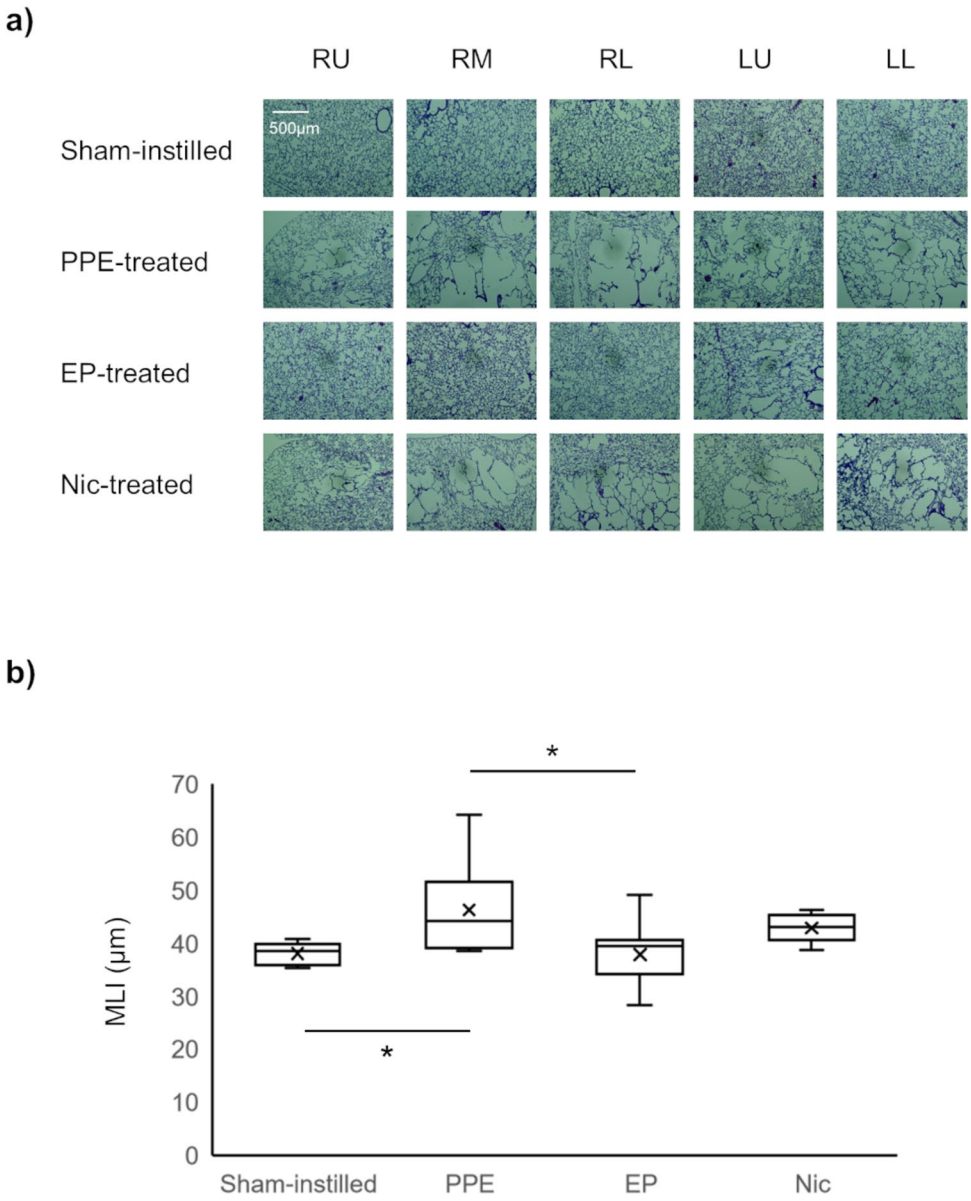

Fig. 4 Representative H&E-stained histology slides obtained from five lung regions of a mouse from each of the four groups, from top to bottom: sham-instilled; PPE-treated; EP-treated; Nic-treated (**a**). *RU*, right upper lobe; *RM*, right middle lobe; *RL*, right lower lobe; *LU*, upper region of the left lobe; *LL*, lower region of the left lobe. Box plots of mean MLI values obtained from mice of each of the four groups (**b**)

a mouse model of elastase-induced lung injury, we reported temporal changes in alveolar septal wall thickness *in vivo* (Figure E5 of Ref. [29]). In this study, significant thickening of the alveolar septal walls was observed *in vivo* on day 1 after PPE administration, prior to the development of emphysema on day 7. In addition, no alveolar septal wall thickening was observed *in vivo* on day 7 after PPE administration. This study supports these assumptions. Notably, in addition to inflammation, a reduction in alveolar tissue volume was reported one day after PPE administration [29]. This finding suggests that, in the present study, tissue destruction to some extent might have already started on day 1 after PPE administration, which is supported by shifts in f_D values caused by PPE administration (Fig. 3). When compared with the f_D values of a sham-instilled mouse on day 0, the f_D values of a PPE-treated mouse on day 1 showed a wider distribution and tended to shift to lower values, similar to that of a PPE-treated mouse on day 21. Therefore, to observe therapeutic effects, it is rational to initiate EP and Nic treatment one day after PPE administration as a significant decrease in f_D value was observed at this time point in the present study.

The decrease in f_D value of the PPE-treated group was consistent from day 1 to day 21 after PPE administration (Fig. 1). As mentioned above, emphysema develops seven days after PPE administration [29]. Therefore, the decrease in f_D value on day 7 after PPE administration was due to the early onset of emphysematous lesions. In contrast, the r_a value of the PPE-treated group was significantly lower than that of the sham-instilled group on day 14 after PPE

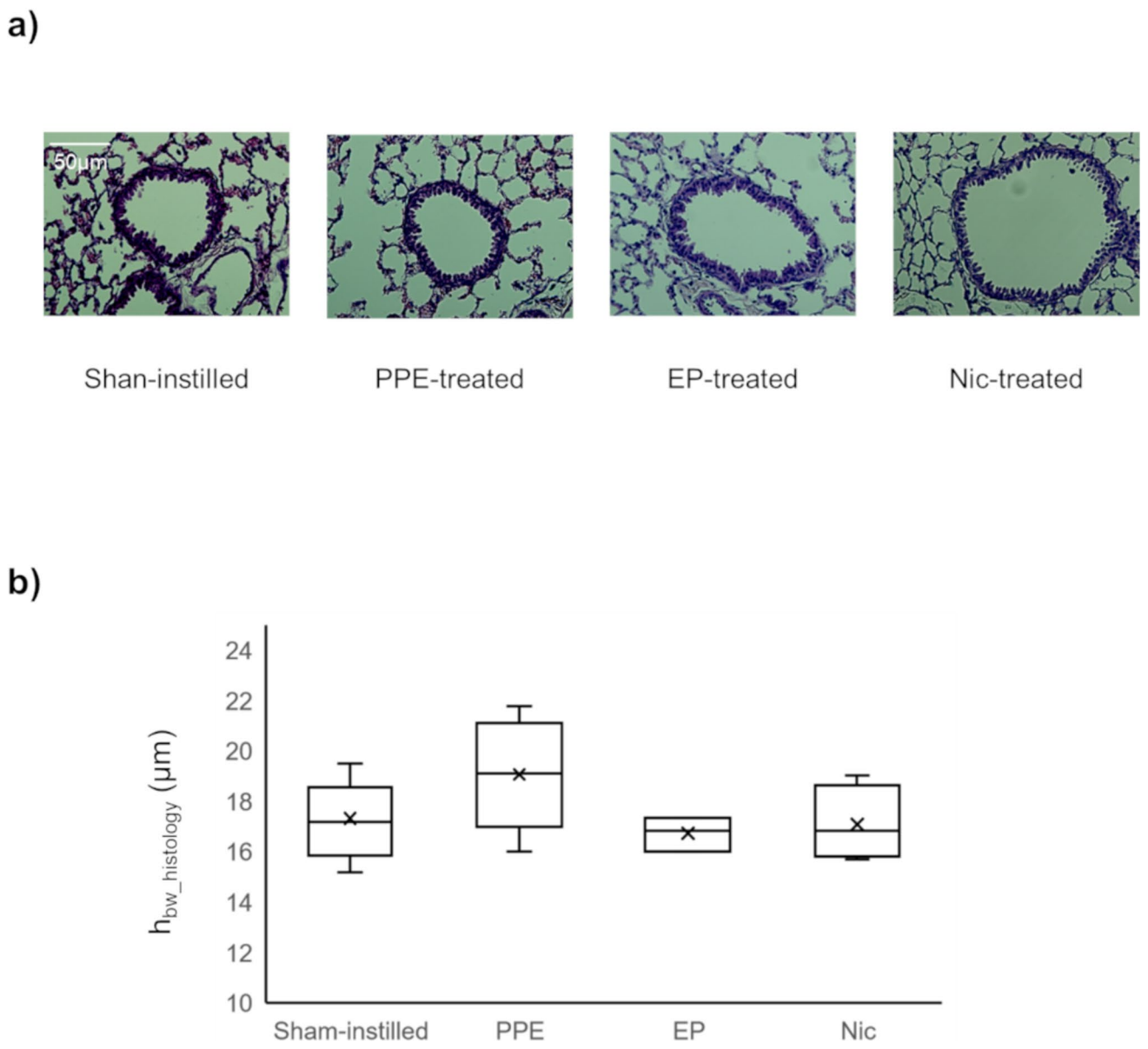

Fig. 5 Representative H&E-stained histology slides obtained from the four groups, from left to right: sham-instilled; PPE-treated, EP-treated; Nic-treated (**a**). Box plots showing the mean bronchial wall thickness ($h_{bw\_histology}$) values obtained from mice of each of the four groups

administration (Fig. 2), implying that emphysematous lesions fully developed at this time point. In contrast, the r_a value of the EP-treated group was higher than that of the Nic-treated groups on day 14 after PPE administration and recovered to a level similar to that of the sham-instilled group, similar to that of f_D value (Figs. 1 and 2). The recovery of both f_D and r_a continued until day 21 after PPE administration, and the MLI of the EP-treated group was significantly lower than that of the PPE-treated group (Fig. 4). Therefore, these data suggest that by starting EP treatment one day after PPE administration, decline in pulmonary function associated with the onset of emphysematous lesions could be improved, as measured by HP ^{129}Xe MRI. However, in the Nic-treated group, the decline in the r_a and f_D values did not improve (Figs. 1 and 2). Moreover, the MLI of the Nic-treated group did not improve compared with that of the PPE-treated group (Fig. 4), supporting the results of the pulmonary functional assessments.

Regulation of the MAPK/ERK pathway has been reported to promote tissue repair during cutaneous wound healing [20]. The MAPK/ERK pathway has been reported to be activated during wound healing in a murine diabetic wound model [21]. Regulation of HMGB1 expression has been reported to be involved in wound healing process via the MAPK/ERK pathway [22]. Based on these reports, we hypothesize that EP regulates the expression levels of

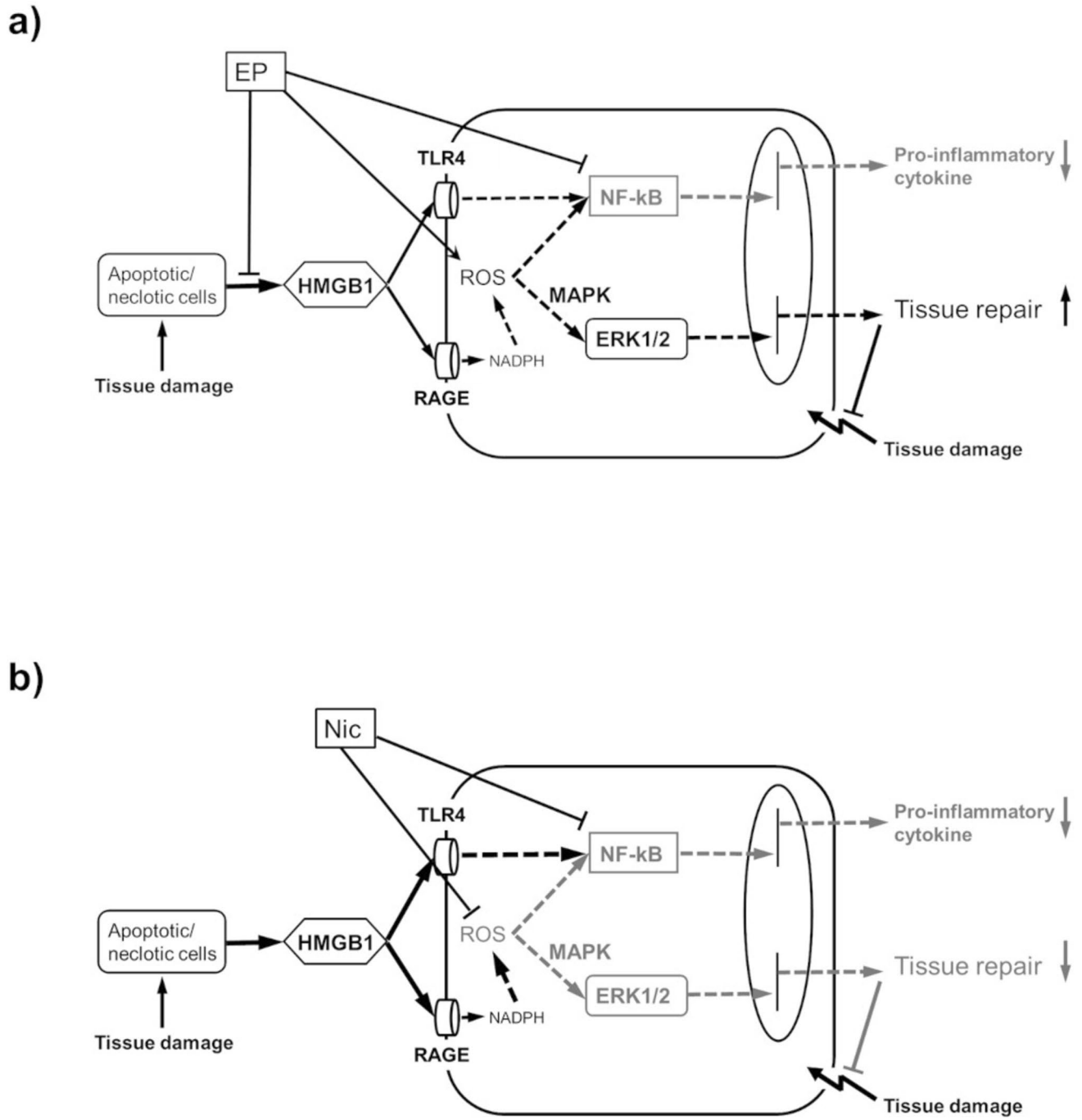

Fig. 6 Proposed mechanisms of therapeutic effect of EP against elastase-induced lung injury. **a**) EP downregulates HMGB1 expression and moderately activates intracellular ROS and MAPK/ERK pathway, thereby initiating wound healing process. **b**) Nic, which inhibits intracellular ROS and deactivates the MAPK/ERK pathway, does not exhibit a positive therapeutic effect

HMGB1 and the MAPK/ERK pathway to exert anti-inflammatory and tissue repair effects. Our previous study using a mouse model of bleomycin-induced lung injury supported this hypothesis, in which we observed lung structural and functional changes caused by the upregulation and downregulation of HMGB1 expression [9]. However, in this study, we were unable to directly elucidate the involvement of intracellular ROS and MAPK/ERK pathway in the recovery of injured tissue.

In the present study, we investigated the involvement of intracellular ROS and MAPK/ERK pathway in elastase-induced emphysema in mice by evaluating and comparing

the pharmacological effects of EP and Nic. Intracellular ROS production has been reported to contribute to elastase-induced lung injury [30]. Further, HMGB1 and NF-kB have also been reported to be involved in elastase-induced lung injury [31, 32]. Furthermore, EP activated the ROS-MAPK/ERK pathway to inhibit melanogenesis in B16F10 melanoma cells [27]. Therefore, we hypothesized that EP moderately upregulates the expression levels of HMGB1 and activates the ROS-MAPK/ERK pathway to exert anti-inflammatory and tissue repair effects (Fig. 6a). In contrast, Nic suppressed ROS production and showed its protective effect through downregulation of the NF-kB and MAPK pathways (Fig. 6b) [28]. In the present study, Nic treatment did not improve pulmonary function, indicating the role of the MAPK/ERK pathway in wound healing process. In other words, non-activation of the MAPK/ERK pathway by Nic treatment seemed to impair tissue repair and lead to the development of emphysema and pulmonary functional decline.

Although Nic has been reported to show protective effects against acute lung injury [28], collapse-induced lung injury [33], pulmonary fibrosis [34, 35], pulmonary artery endothelial damage in pulmonary hypertension [36], and other lung disorders [37], its therapeutic effects have not been reported. In the present study, inflammation was detected one day after PPE administration, and Nic treatment was started at this stage to suppress the inflammation through inhibition of intracellular ROS production and NF-kB activation [28]. However, at this stage, in addition to inflammation, there appeared to be some extent of tissue destruction, as mentioned previously. We assumed that Nic did not show tissue repair effects via the MAPK/ERK pathway and was unable to exert a therapeutic effect considering the above reason. In contrast, EP downregulated HMGB1 expression, increased ROS production, and moderately upregulated the MAPK/ERK pathway (Fig. 6a) [24–27], resulting in tissue repair and suppression in the onset of emphysema, leading to improvement in pulmonary function.

Finally, owing to the limited sample size of this study, the observed associations between lung function parameters (f_D and r_a) obtained from HP ^{129}Xe MRI and the treatment effects of EP and Nic should be interpreted with caution. Further validation using a larger cohort is required to confirm these findings.

Conclusions

In the present study, we successfully monitored temporal changes in pulmonary function of gas exchange and ventilation caused by the development of emphysema using a preclinical HP ^{129}Xe MRI protocol. The treatment responses of EP and Nic against the development of emphysema were monitored and compared. EP treatment effectively repaired tissue damage and improved pulmonary function in elastase-induced lung injury, whereas Nic showed no therapeutic effects. The present results suggest therapeutic efficacy of EP in wound healing process via activation of the MAPK/ERK pathway.

Supplementary Information The online version contains supplementary material available at https://doi.org/10.1007/s11307-025-02073-6.

Acknowledgements The authors are grateful to all members of the Department of Medical Physics and Engineering, Area of Medical Imaging Technology and Science, Division of Health Sciences, Graduate School of Medicine, The University of Osaka, for their valuable comments and helpful discussions. The authors would like to thank Editage (www.editage.jp) for English language editing.

Author Contributions Atsuomi Kimura designed the study. Material preparation, data collection, and analysis were conducted by all the authors. Atsuomi Kimura wrote the first draft of the manuscript. All authors have read and approved the final manuscript.

Funding This work was supported in part by the Grant-in-Aids of Scientific Research (No. 20H04516) from the Ministry of Education, Culture, Science, Sports, and Technology of Japan.

Data Availability The datasets generated in this study are available from the corresponding author upon reasonable request.

Declarations

Ethical Approval The animal study protocol was approved by the Institutional Animal Care and Use Committee of Division of Health Sciences, Graduate School of Medicine, The University of Osaka (approval no. 24–03-03).

Conflicts of interest The authors declare that they have no conflict of interest.

References

1. MacLeod JL, Khan HM, Franklin A, Myc L, Shim YM (2025) Hyperpolarized xenon-129 MRI: narrative review of clinical studies, testing, and implementation of advanced pulmonary *in vivo* imaging and its diagnostic applications. Diagnostics 15:474
2. Niedbalski PJ, Hall CS, Castro M et al (2021) Protocols for multi-site trials using hyperpolarized ^{129} Xe MRI for imaging of ventilation, alveolar-airspace size, and gas exchange: A position paper

from the ^{129} Xe MRI clinical trials consortium. Magn Reson Med 86:2966–2986
3. Stewart NJ, Smith LJ, Chan HF et al (2022) Lung MRI with hyperpolarised gases: current & future clinical perspectives. Br J Radiol 95:20210207
4. Zhang Z, Li H, Xiao S et al (2024) Hyperpolarized gas imaging in lung diseases: functional and artificial intelligence perspective. Acad Radiol 31:4203–4216
5. Imai H, Kimura A, Hori Y et al (2011) Hyperpolarized 129Xe lung MRI in spontaneously breathing mice with respiratory gated fast imaging and its application to pulmonary functional imaging. NMR Biomed 24:1343–1352
6. Imai H, Matsumoto H, Miyakoshi E et al (2015) Regional fractional ventilation mapping in spontaneously breathing mice using hyperpolarized ^{129}Xe MRI. NMR Biomed 28:24–29
7. Fukui E, Funaki S, Kimura K et al (2019) Adipose tissue-derived stem cells have the ability to differentiate into alveolar epithelial cells and ameliorate lung injury caused by elastase-induced emphysema in mice. Stem Cells Int 2019:5179172
8. Kimura A, Yamauchi Y, Hodono S et al (2017) Treatment response of ethyl pyruvate in a mouse model of chronic obstructive pulmonary disease studied by hyperpolarized ^{129} Xe MRI. Magn Reson Med 78:721–729
9. Hodono S, Shimokawa A, Stewart NJ et al (2018) Ethyl pyruvate improves pulmonary function in mice with bleomycin-induced lung injury as monitored with hyperpolarized ^{129}Xe MR imaging. Magn Reson Med Sci 17:331–337
10. Kimura A, Utsumi S, Shimokawa A et al (2021) Inflammation during lung cancer progression and ethyl pyruvate treatment observed by pulmonary functional hyperpolarized ^{129}Xe MRI in mice. Contrast Media Mol Imaging 2021:9918702
11. Yang Q, Li M, Hou Y, He H, Sun S (2023) High-mobility group box 1 emerges as a therapeutic target for asthma. Immun Inflamm Dis 11:e1124
12. Furci F, Murdaca G, Pelaia C et al (2023) TSLP and HMGB1: inflammatory targets and potential biomarkers for precision medicine in asthma and COPD. Biomedicines 11:437
13. Wulandari S, Hartono WT (2023) The role of HMGB1 in COVID-19-induced cytokine storm and its potential therapeutic targets: A review. Immunology 169:117–131
14. Lin L, Li J, Song Q, Cheng W, Chen P (2022) The role of HMGB1/RAGE/TLR4 signaling pathways in cigarette smoke-induced inflammation in chronic obstructive pulmonary disease. Immun Inflamm Dis 10:e711
15. Zhang Y, Li S, Wang G et al (2014) Changes of HMGB1 and sRAGE during the recovery of COPD exacerbation. J Thorac Dis 6:734–741
16. Wang H, Yang H, Czura CJ, Sama AE, Tracey KJ (2001) HMGB1 as a late mediator of lethal systemic inflammation. Am J Respir Crit Care Med 164:1768–1773
17. Coughlan MT, Thorburn DR, Penfold SA et al (2009) RAGE-induced cytosolic ROS promote mitochondrial superoxide generation in diabetes. J Am Soc Nephrol 20:742–752
18. Lingappan K (2018) NF-κB in oxidative stress. Curr Opin Toxicol 7:81–86
19. Son Y, Cheong YK, Kim NH et al (2011) Mitogen-activated protein kinases and reactive oxygen species: how can ROS activate MAPK pathways? J Signal Transduct 792639. https://doi.org/10.1155/2011/792639
20. Escuin-Ordinas H, Li S, Xie MW et al (2016) Cutaneous wound healing through paradoxical MAPK activation by BRAF inhibitors. Nat Commun 7:12348
21. Escuin-Ordinas H, Liu Y, Sun L et al (2021) Wound healing with topical BRAF inhibitor therapy in a diabetic model suggests tissue regenerative effects. PLoS ONE 16:e0252597
22. Lee DE, Trowbridge RM, Ayoub NT, Agrawal DK (2015) High-mobility group box protein-1, matrix metalloproteinases, and vitamin D in keloids and hypertrophic scars. Plast Reconstr Surg Glob Open 3:e425
23. Yamaguchi K, Iwamoto H, Sakamoto S et al (2020) Serum high-mobility group box 1 is associated with the onset and severity of acute exacerbation of idiopathic pulmonary fibrosis. Respirology 25:275–280
24. Yu Y, Yu Y, Liu M et al (2016) Ethyl pyruvate attenuated coxsackievirus B3-induced acute viral myocarditis by suppression of HMGB1/RAGE/NF-KB pathway. Springerplus 5:215
25. Fan R, Wang L, Botchway BOA, Zhang Y, Liu X (2022) Protective role of ethyl pyruvate in spinal cord injury by inhibiting the high mobility group box-1/toll-like receptor4/nuclear factor-kappa B signaling pathway. Front Mol Neurosci 15:1013033
26. Kung CW, Lee YM, Cheng PY, Peng YJ, Yen MH (2011) Ethyl pyruvate reduces acute lung injury via regulation of iNOS and HO-1 expression in endotoxemic rats. J Surg Res 167:e323–e331
27. Zhou S, Sakamoto K (2019) Pyruvic acid/ethyl pyruvate inhibits melanogenesis in B16F10 melanoma cells through PI3K/AKT, GSK3β, and ROS-ERK signaling pathways. Genes Cells 24:60–69
28. He M, Shi W, Yu M et al (2019) Nicorandil attenuates LPS-induced acute lung injury by pulmonary endothelial cell protection via NF-κB and MAPK pathways. Oxid Med Cell Longev. https://doi.org/10.1155/2019/4957646
29. Tetsumoto S, Takeda Y, Imai H et al (2013) Validation of non-invasive morphological and diffusion imaging in mouse emphysema by micro-computed tomography and hyperpolarized (129) Xe magnetic resonance imaging. Am J Respir Cell Mol Biol 49:592–600
30. Tanaka KI, Shiota S, Sakakibara O et al (2022) Exacerbation of elastase-induced emphysema via increased oxidative stress in metallothionein-knockout mice. Biomolecules 12:583
31. Pouwels SD, Hesse L, Wu X et al (2021) LL-37 and HMGB1 induce alveolar damage and reduce lung tissue regeneration via RAGE. Am J Physiol Lung Cell Mol Physiol 321:L641–L652
32. Suraya R, Nagano T, Ryanto GRT et al (2022) Budesonide/glycopyrronium/formoterol fumarate triple therapy prevents pulmonary hypertension in a COPD mouse model via NFκB inactivation. Respir Res 23:173
33. Wang C, Ke H, Xu X et al (2019) Protective effect of nicorandil on collapse-induced lung injury in rabbits by inhibiting apoptosis. Int J Mol Med 44:725–736
34. Kseibati MO, Shehatou GSG, Sharawy MH, Eladl AE, Salem HA (2020) Nicorandil ameliorates bleomycin-induced pulmonary fibrosis in rats through modulating eNOS, iNOS, TXNIP and HIF-1α levels. Life Sci 246:117423
35. El-Kashef DH (2018) Nicorandil ameliorates pulmonary inflammation and fibrosis in a rat model of silicosis. Int Immunopharmacol 64:289–297
36. Wang H, Zuo X, Wang Q et al (2013) Nicorandil inhibits hypoxia-induced apoptosis in human pulmonary artery endothelial cells through activation of mitoKATP and regulation of eNOS and the NF-κB pathway. Int J Mol Med 32:187–194
37. Ahmed LA, El-Maraghy SA, Rizk SM (2015) Role of the KATP channel in the protective effect of nicorandil on cyclophosphamide-induced lung and testicular toxicity in rats. Sci Rep 5:14043